Two Biochemical Oscillators Coupled by Mass Exchange

A. Lekebusch and F. W. Schneider*

Institute of Physical Chemistry, University of Würzburg, Am Hubland, D-97074 Würzburg, Germany

Received: July 11, 1997; In Final Form: September 2, 1997[⊗]

We present experiments and simulations of two mutually mass-coupled biochemical oscillators represented by the nonlinear peroxidase-oxidase reaction. The uncoupled oscillators show simple period-1 (P1) oscillations of different frequencies for different values of the oxygen concentration in the gas stream. A phase diagram is established where the ratio of the natural frequencies is plotted versus the mass exchange rate. For each frequency ratio four regimes of behavior have been observed for an increasing mass exchange rate: (I) two independent and uncorrelated P1 oscillations; (II) quasiperiodicity in one and P1 oscillations in the other reactor; (III) quasiperiodicity in both reactors; (IV) periodic in-phase synchronization of both reactors. We use the correlation coefficient, the frequencies of the system, and the phase difference between the two cells to characterize the four regimes. A new feature of this work is the experimental observation of an "infinite" modulation period at the transition from the quasiperiodic region to the limit cycle that can be explained by a collision of a torus with a saddle-node bifurcation of a limit cycle (SNIPER bifurcation of codimension two). Simulations using two coupled four-variable DOP models give very good agreement with the experimental results and support our interpretation of the dynamical behavior and the observed bifurcations.

I. Introduction

Coupled chemical oscillators have been the subject of many investigations, since they may serve as models for coupled biological systems. For example, the cell-to-cell coupling of sinus node cells is responsible for triggering the heartbeat[1] and coupling is important in numerous transformation processes in living cells, tissues, and networks of neurons.

Nonlinear chemical oscillators can be coupled by various methods, including mass-exchange,[2−8] flow-rate coupling[9−12] or electrical coupling.[13−15] Mass coupling is the most common method; it has been intensively studied in the Belousov−Zhabotinsky reaction. Marek and Stuchl coupled two stirred tank reactors (CSTRs) by mass transfer through a perforated wall.[2] They found entrainment of oscillations when the natural frequencies of the uncoupled BZ oscillators had ratios near 1:1, 1:2, 1:3, etc. Fujii and Sawada[4] and Nakajima and Sawada[5] constructed a phase diagram (oscillation frequency vs coupling strength) of the dynamical behavior of two BZ oscillators coupled by mass transfer. Linear arrays of several coupled reactors were investigated by Stuchl and Marek (seven reactors; BZ reaction)[16] and by Laplante and Erneux (16 reactors; chlorite−iodide reaction).[17] Coupling via mass transfer can cause a pair of oscillators to reach a stable steady state. This phenomenon was called phase death by Bar-Eli who investigated several models of chemical oscillators and analyzed the obtained steady states.[18] Crowley and Epstein analyzed the experimental steady states emerging through phase death by the coupling of two nearly identical BZ oscillators.[6] The coupling of two Brusselator models was the subject of a number of investigations.[19−22]

Here, we describe the effect of two mass-coupled biochemical oscillators using the peroxidase−oxidase (PO) reaction. The dependence of the ratio of the natural frequencies on the mass exchange rate is represented by a bifurcation diagram. We discuss the route from the uncoupled (no mass exchange) to the highly coupled reactors. The appearance of quasiperiodicity and its bifurcation to a stable limit cycle via a SNIPER (**s**addle **n**ode **i**nfinite **per**iod) bifurcation of codimension two will be shown. The experimental results are compared with calculations using the four-variable model of Degn, Olsen, and Perram (DOP).[23]

II. PO Reaction

The PO reaction is the aerobic oxidation of the reduced form of nicotineamide adenine dinucleotide (NADH) catalyzed by the enzyme horseradish peroxidase (HRP).

$$2\mathrm{NADH} + \mathrm{O_2} \xrightarrow{[\mathrm{HRP}]} 2\mathrm{NAD^+} + \mathrm{H_2O} \qquad (1)$$

NAD^+ is β-nicotineamide adenine dinucleotide also known as coenzyme 1. Chemical recycling may be achieved by another enzyme reaction

$$\mathrm{NAD^+} + \mathrm{G6P} \xrightarrow{[\mathrm{DH}]} \mathrm{6PGL} + \mathrm{NADH} + \mathrm{H^+} \qquad (2)$$

where DH is glucose 6-phosphate dehydrogenase. The substrate for the second enzyme is glucose 6-phosphate (G6P), which is oxidized to 6-phosphoglucolactone (6PGL).

The experimental conditions are chosen in such a way that for the free-running system only P1 oscillations are observed at all flow-rates. The bifurcation diagram is shown in Figure 1 where the bifurcation parameter is the oxygen concentration in the gas stream.

III. Experimental Section

Reactor. Two CSTRs (**c**ontinuous flow **s**tirrred **t**ank **r**eactor) made from Plexiglas were used (Figure 2). Each CSTR had a square base of 18 mm width and 18 mm height with an effective liquid volume of 4.3 mL. The gas volume above the liquid was 2.0 mL. We used nonsymmetric stirrers (each a mirror image of the other) of about 1.5 mL self-volume, which were driven by small motors with a stirring rate of 1500 rpm. This was found to be a good combination of efficient mixing of the liquid and a constant oxygen-transfer rate through the liquid surface. Initial experiments did not show any difference

* To whom correspondence should be addressed.
[⊗] Abstract published in *Advance ACS Abstracts,* October 15, 1997.

S1089-5647(97)02257-8 CCC: $14.00

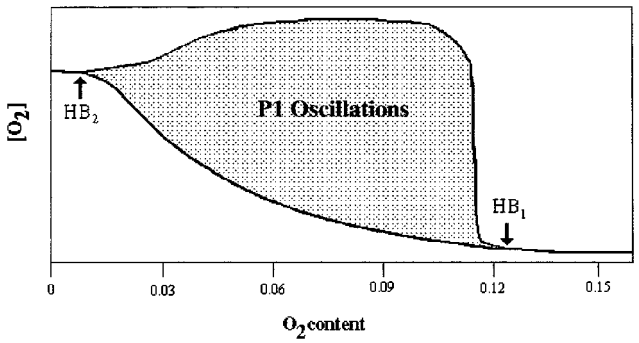

Figure 1. Experimental bifurcation diagram at pH = 5.5 as a function of O_2 content in the gas mixture.

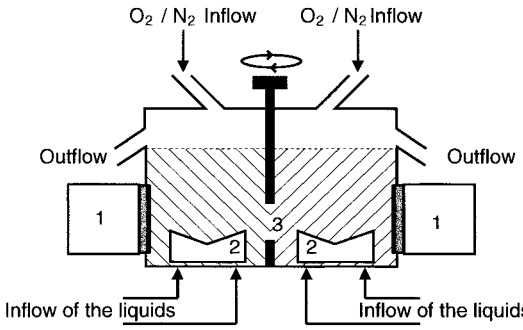

Figure 2. Two CSTRs with 4.2 mL volume each. Each CSTR has two inlets for the liquid reactants, a gas inlet, and a gas/liquid outlet. The CSTRs are monitored with O_2 Clark electrodes (1). Each reactor is magnetically stirred at 1500 rpm (2). Mass exchange is realized by a variable orifice (3).

between symmetric and nonsymmetric stirring at the high and efficient stirring rate used in the experiments, i.e., CSTR boundary conditions were maintained throughout our experiments. The use of nonsymmetric stirring is therefore fortuitous. The oxygen-transfer rate was determined to be 1.11×10^{-3} s^{-1} at 25 °C. The mass exchange was realized by an orifice in the common reactor wall between the two CSTRs. Its size could be varied by a screw to regulate the mass exchange rate, which varied between 0 and 1.5×10^{-2} s^{-1}. The outflow of the liquids was regulated to avoid a net mass flow through the two CSTRs.

Materials. Peroxidase from horseradish (HRP, RZ 3.05, acitivity 270 units per mg of solid) was purchased from Sigma as a salt-free powder. Glucose 6-phosphate dehydrogenase (DH) from leuconostic mesenteroides (540 units β-NAD^+ per mg of protein) was purchased from Sigma as a biuret suspension. β-NAD^+ from yeast (99%) and D-glucose 6-phosphate disodium salt (G6P, 99%) were purchased from Sigma. 2,4-Dichlorophenole and methylene blue were purchased from Aldrich.

Preparation of Inflow Components. All reactants were dissolved in aqueous 0.1 M phosphate buffer (pH 5.8) containing 1 mmol/L methylene blue and 50 mmol/L 2,4-dichlorophenole. We used two syringes (Hamilton) filled with NAD^+/G6P solution and DH/HRP solution, respectively, containing the following concentrations: (syringe 1) 3.0 mmol/L [NAD^+], 50 mmol/L [G6P]; (syringe 2) 100 units/mL [HRP], 5.0 units/mL [DH]. All experiments were carried out at 25 °C, pH 5.5.

Continuous Flow Conditions. A self-designed high-precision syringe pump driven by a computer-linked stepping motor was employed to control the flow rate of the reactants into the CSTR. The stepping frequency was 10 Hz, producing a constant flow rate of the two solutions at k_f(liquid) = 1.3×10^{-4} s^{-1} (residence time τ = 128 min). For each cell two mass-flow controllers (MKS Type 1259C) were used for mixing O_2 and N_2 at defined ratios and for regulating the gas flow rate. The

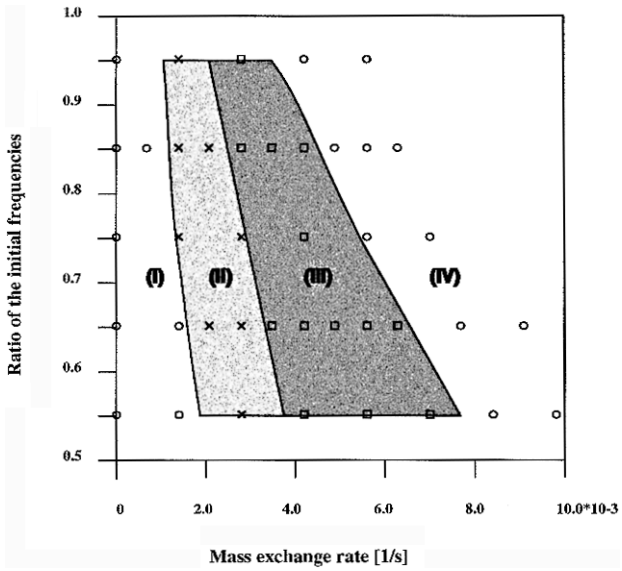

Figure 3. Experimental phase diagram showing the ratio of the natural frequencies ω_2/ω_1 versus the mass exchange rate D between the two reactors: (I) independent oscillatory behavior P1 in both cells; (II) one reactor is quasiperiodic, the other shows a P1 oscillation; (III) both reactors are quasiperiodic; (IV) both reactors show in-phase entrainment.

flow rate of the gaseous O_2/N_2 mixture was different for each cell, but it was held constant during the experiment.

Detection. The time series of the oxygen concentration in solution was measured with an oxygen-selective Clark electrode with a sampling rate of 1 Hz.

IV. Results

Experiments. The mass-transfer experiments include two limiting cases, namely, zero and infinite coupling. At zero coupling the two reactors show independent oscillatory behavior where the two frequencies depend on the bifurcation parameter (oxygen concentration in the gas stream). At very high coupling strength there is enough mass transfer to equalize the concentrations of all species in the two reactors. Thus, the system acts like one reactor with two inflows. In the experimental phase diagram the ratio of the natural frequencies ω_2/ω_1 is plotted versus the mass transfer rate D (Figure 3). The diagram is divided into four regions. (I) For zero and for small mass exchange rates the oscillators show independent P1 oscillations. (II) With increasing coupling strength a new frequency is observed in the first reactor, while the second reactor still shows P1 oscillations. The new frequency is equal to the main P1 frequency in the second reactor. The existence of two incommensurate frequencies in the first reactor corresponds to quasiperiodic behavior. (III) This region is characterized by the appearance of a second frequency in the second reactor. Here, both oscillators oscillate quasiperiodically. The quasiperiodicity in both reactors has one common frequency. The modulation frequencies corresponding to the absolute differences between the two frequencies in each cell are equal. (IV) Very high mass exchange rates lead to synchronization of the two reactors. It is seen that the final frequency is equal to the natural frequency of the first reactor. This indicates that the higher frequency oscillator has entrained the lower frequency oscillator.

Examples of the four regions are shown in parts 4.1−4.4 of Figure 4 for a ratio of the natural frequencies of $\omega_2/\omega_1 = 0.65$. In the time series reactor 1 is represented by a solid curve and reactor 2 by a dotted curve. The temporary evolution of the phase difference between the two reactors is shown in parts 4.1b−4.4b. In region I the oscillators are independent and the

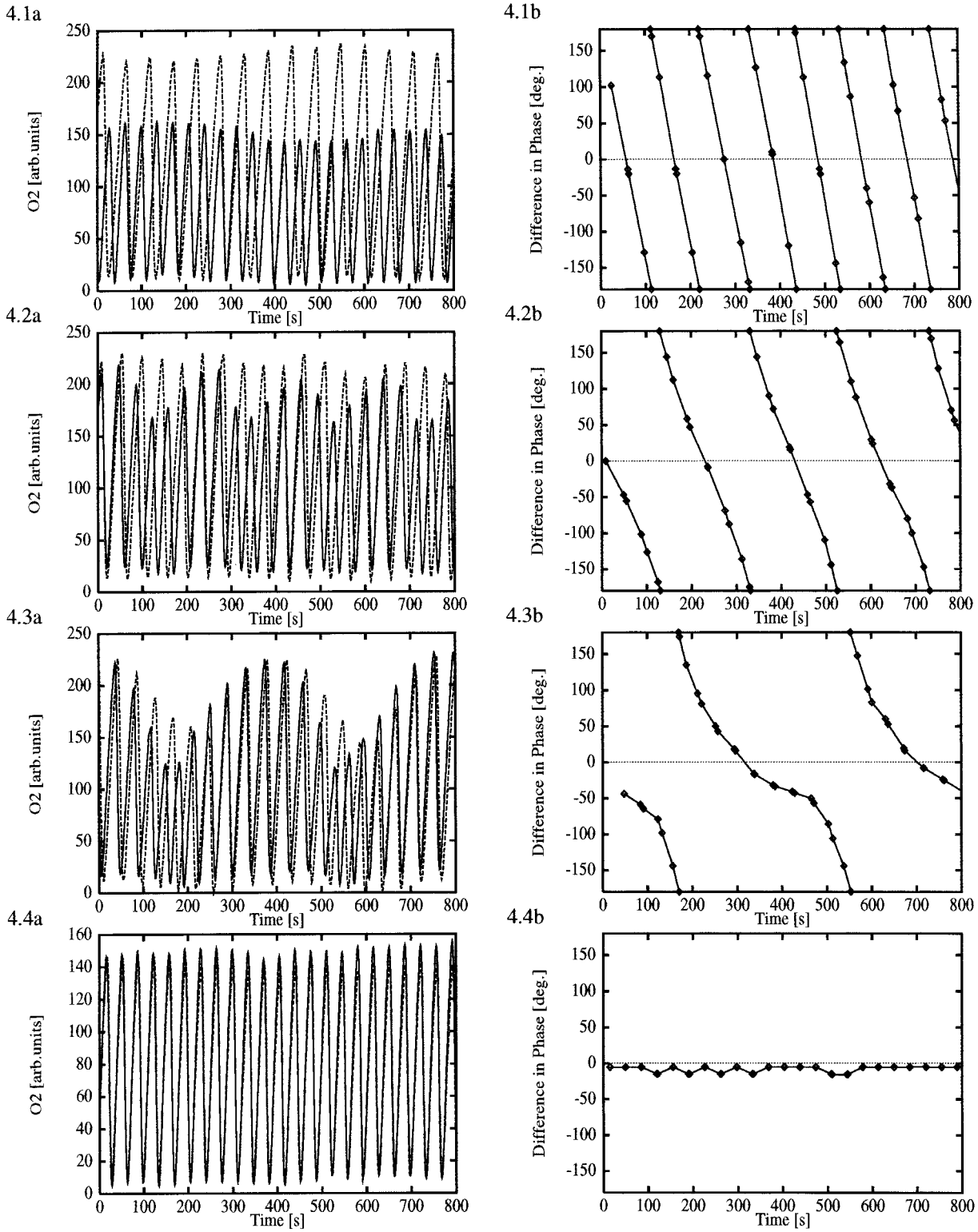

Figure 4. (4.1a−4.4a) Experimental time series (CSTR 1, solid line; CSTR 2, dotted line) and (4.1b−4.4b) phase-difference as a function of time at different mass exchange rates at a ratio of the natural frequencies of $\omega_2/\omega_1 = 0.65$: (4.1) $D = 0$; (4.2) $D = 2.8$ 1/s; (4.3) $D = 4.9$ 1/s; (4.4) $D = 7.7$ 1/s.

phase difference varies linearly with time between +180 and −180° (Figure 4.1). Mass coupling in regions II and III causes the phase difference to deviate from linear behavior (parts 4.2 and 4.3 of Figure 4). Mass exchange leads to a partial synchronization of the oscillators. For strong mass coupling (region IV) reactors 1 and 2 are in phase (Figure 4.4).

The evolution of the main frequencies as determined by the experimental Fourier spectra is shown in Figure 5. For low mass exchange rates ($D = 0-0.0014$ s^{-1}, region I) a shift of the initial frequencies is observed. A second frequency appears in reactor 1 (faster oscillator) at $D = 0.0021$ s^{-1} (region II), which is equal to the P1 frequency of reactor 2. Quasiperiodicity is indicated by two incommensurate frequencies. In experiments it is difficult to distinguish between noisy P1 oscillations and quasiperiodic oscillations of small modulation amplitudes. An experimental distinction can be made if the amplitude of the second frequency is at least ∼20% of the amplitude of the first frequency. Quasiperiodicity can be observed in both reactors ($D = 0.0035$ s^{-1}) in region III where both reactors have a common frequency. Interestingly, a

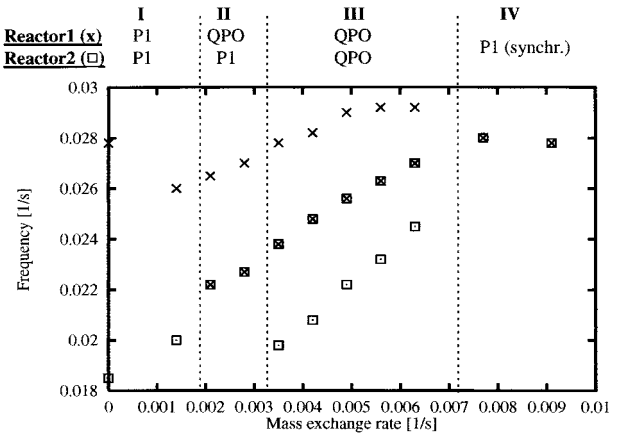

Figure 5. Frequencies of both reactors as a function of mass exchange rate (ratio of the natural frequencies $\omega_2/\omega_1 = 0.65$). This experimental diagram is divided in four regions (see Figure 3).

positive and a negative linear combination of the common frequency with the modulation frequency is observed in reactors 1 and 2, respectively. A further increase of the coupling strength leads to a decrease of the modulation frequency (Figure 6). At $D = 0.007\ s^{-1}$ the modulation frequency of the quasiperiodicity tends to zero in both reactors. For mass exchange rates $D > 0.007\ s^{-1}$ both reactors display the same frequency, which corresponds to the natural frequency of the faster oscillator.

Calculations. Computer simulations were performed using the four-variable model of Degn, Olsen, and Perram (DOP).[23] The variables are A = O_2, B = NADH; X and Y are radical intermediates. The basic model, all rate constants, and initial conditions are given in Table 1.

The free-running system shows P1 oscillations over a wide range of the bifurcation parameter k_7, which represents the transport of gaseous oxygen into the reaction solution. The observed species is A. Two sets of DOP models are used with coupling terms[3] included as follows:

$$\frac{dc_i^k}{dt} = f_i(c_1^k, ..., c_n^k; p^k) + \sum_{j=1}^{n} d_{ij} \sum_{l=1}^{N} \delta^{lk}(c_j^l - c_j^k) \qquad (3)$$

for

$$i = 1, ..., n$$

$$k = 1, ..., N$$

$$n = 4$$

$$N = 2$$

where c_i^k is the concentration of the ith chemical component in the kth cell. The reaction kinetics and the CSTR boundary conditions (dependent on a set of parameters p^k) are contained in f_i. The rate of transport of the ith component between the cells is proportional to the difference of the respective concentrations. Here, we present simulations with a symmetric coupling function $\delta^{12} = \delta^{21} = 1$. For all variables of the system equal exchange rates $d_{11} = d_{22} = d_{33} = d_{44} = D$ are used. The initial conditions of the two cells (autonomous system for $D = 0$) are chosen such that both cells have single stable periodic states with different frequencies as in the experiments. In the second cell a periodic orbit with a frequency of $\omega = 0.345\ s^{-1}$ is observed for $k_7 = 1.40$, while the frequency of the periodic orbit in the first cell varies between $\omega = 0.347\ s^{-1}$ (at $k_7 = 1.42$) and $\omega = 0.491\ s^{-1}$ (at $k_7 = 3.00$).

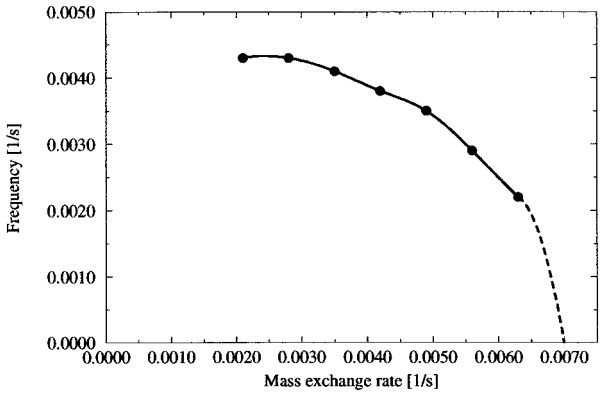

Figure 6. Experimental modulation frequency as a function of mass exchange rate in the quasiperiodic states II and III at a ratio of the natural frequencies $\omega_2/\omega_1 = 0.65$.

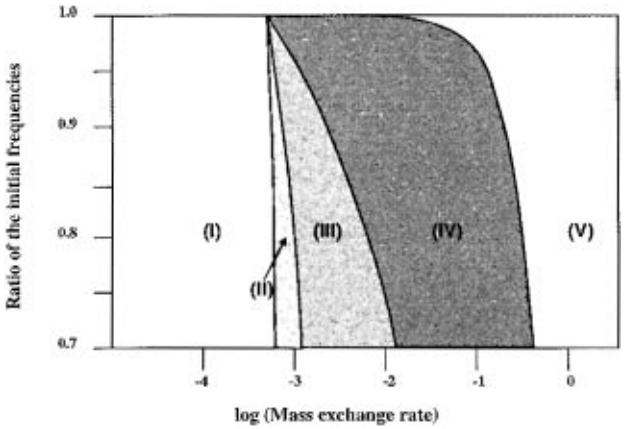

Figure 7. Coupling state diagram of two coupled DOP models: (I) independent P1 oscillatory behavior in both cells; (II) quasiperiodic in one cell, P1 oscillations in the other; (III) both oscillators are quasiperiodic; (IV) out-of-phase entrained oscillators; (V) in-phase entrained oscillators. Note that the out-of-phase entrainment is missing in the experiments (Figure 3).

TABLE 1: DOP Model with Rate Constants and Initial Parameters

	rate constants
$A + B + X \rightarrow 2X$	$k_1 = 0.245$
$2X \rightarrow 2Y$	$k_2 = 1250$
$A + B + Y \rightarrow 2X$	$k_3 = 0.046\,875$
$X \rightarrow P$	$k_4 = 20$
$Y \rightarrow Q$	$k_5 = 1.104$
$[X]_0 \rightarrow X$	$k_6 = 1 \times 10^{-3}$
$[A]_0 \rightleftharpoons A$	$k_7 = 0.79-3.4$; $k_{-7} = 0.1175$
$[B]_0 \rightarrow B$	$k_8 = 0.5$
initial parameters	
	$A_0 = 5.6$
	$B_0 = 2.4 \times 10^1$
	$X_0 = 2.7 \times 10^{-2}$
	$Y_0 = 2.409 \times 10^{-3}$

A phase diagram (Figure 7) shows the results of the calculations when the ratio of the initial frequencies ω_2/ω_1 is plotted versus the mass exchange rate (logarithmic scale). We observe similar dynamic states of the system as in the experiments with a variable exchange rate. For small rates both cells show P1 oscillations (region I). In regions II and III an expansion in volume of a two-torus from the stable limit cycle could be observed. If the Fourier spectrum of the observed variable shows a second frequency whose amplitude is ≥10% of the amplitude of the main frequency, the appearance of a two-torus is indicated. This convention has to be used in order to compare our experiments with the calculations. In the cell

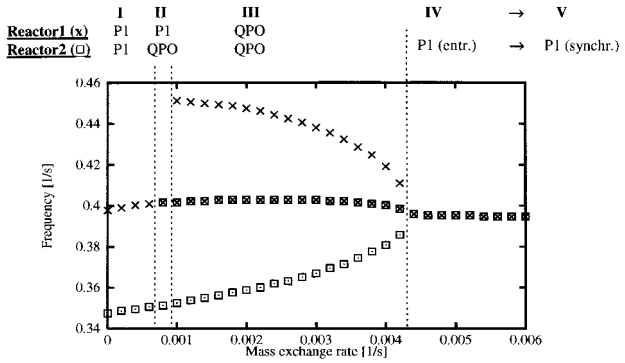

Figure 8. Frequencies of two coupled DOP models as a function of mass exchange rate (ratio of the natural frequencies $\omega_2/\omega_1 = 0.86$).

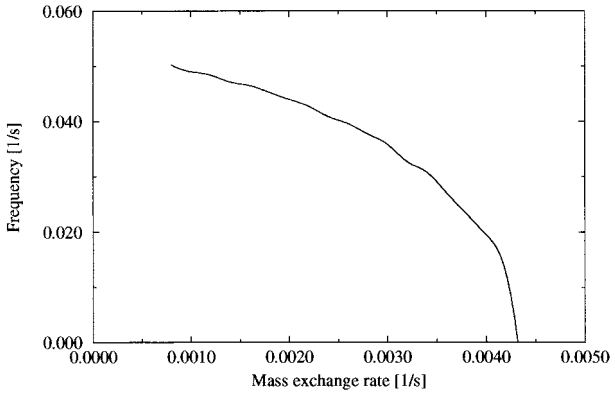

Figure 9. Modulation frequency of two DOP models (ratio of the natural frequencies $\omega_2/\omega_1 = 0.86$) in regions II and III.

with the lower initial frequency the quasiperiodic state is reached first. At high coupling strength (region IV) the two cells show a limit cycle with the same frequency that corresponds to the initial frequency of the faster cell. The oscillators have a phase difference of ∼95°. The phase difference is reduced with increasing exchange rate. At very high mass exchange rates (region V) the concentration difference between the active species disappears and the variables show the same limit cycle (in-phase entrainment).

The evolution of the frequencies (Figure 8) with increasing mass exchange rate show a similar behavior as in our experiments. For small exchange rates ($D = 0-7 \times 10^{-4}$ s^{-1}) we observe a shift of the frequencies without a significant change of the global dynamics (region I; P1 oscillations of different frequencies). The appearance of quasiperiodicity is observed in the cell with the lower frequency at $D = 7 \times 10^{-4}$ s^{-1} and in the higher frequency cell at $D = 9 \times 10^{-4}$ s^{-1}. The bifurcation from region III (quasiperiodic behavior in both cells) to region IV (out-of-phase entrainment of 95°) corresponds to the bifurcation found in our experiments. In simulations and experiments we observe a reduction of the difference between the two main frequencies of the quasiperiodicity (corresponding to an increase of the modulation period of the quasiperiodicity) by approaching the bifurcation point from lower values of the mass exchange rate. At the bifurcation point the modulation frequency tends to zero (Figure 9).

V. Discussion

The coupling of two oscillating biochemical PO oscillators by mass exchange was shown to produce different dynamic states by varying the ratio of the initial frequencies and the mass exchange rate. With increasing mass exchange rate the system shows independent oscillatory, quasiperiodic, and entrained oscillatory behavior with in-phase entrainment in the experiments and both in-phase and out-of-phase entrainment in the simulations depending on the coupling strength. For increasing coupling strength we observed a gradual coalescence of the two frequencies of the quasiperiodic motion in both reactors, since the modulation frequency tended to zero. The more the ratio of the initial frequencies deviates from unity, the larger are the coupling strengths that are required for the coupled oscillators to pass through regions I−IV. Further analysis can be carried out with the correlation coefficient. The correlation coefficient $C(x_{i,k}, x_{i,l})$ is a measure of the linear dependence between two quantities, such as the time series $x_{i,k}$ and $x_{i,l}$. $C(x_{i,k}, x_{i,l})$ is defined as

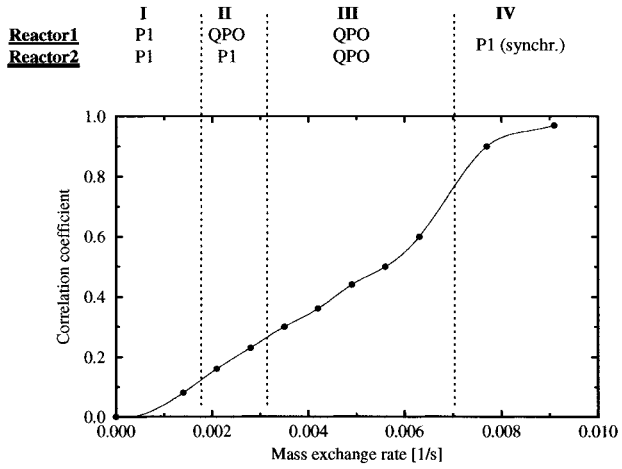

Figure 10. Experimental correlation coefficient C as a function of mass exchange rate at $\omega_2/\omega_1 = 0.65$.

$$C(x_{i,k}, x_{i,l}) = \frac{\sum_i [(x_{i,k} - \bar{x}_k)(x_{i,l} - \bar{x}_l)]}{\sqrt{\sum_i [(x_{i,k} - \bar{x}_k)^2 (x_{i,l} - \bar{x}_l)^2]}} \qquad (4)$$

$C(x_{i,k}, x_{i,l})$ varies between −1 and 1. For $C(x_{i,k}, x_{i,l}) = 1$ the compared time series oscillate in-phase with the same frequency. $C(x_{i,k}, x_{i,l}) = -1$ indicates an out-of-phase correlation. Linearly independent time series cannot be distinguished from entrained times series whose phase difference is 90 or 270° by the correlation coefficient because both cases lead to $C(x_{i,k}, x_{i,l}) = 0$.

In our context we use the correlation coefficient $C(x_{i,k}, x_{i,l})$ to analyze the transition between the uncoupled ($D = 0$) and the highly coupled systems ($D > 7 \times 10^{-2}$ s^{-1}). $C(x_{i,k}, x_{i,l})$ increases continuously with increasing mass transfer rate (Figure 10). This shape is the result of a continuous stabilization of both reactors in a synchronized state. Four examples of the evolution of this state are shown in the time series and the corresponding phase-difference plots in Figure 4. A complete development of the evolution of the phase difference with time is demonstrated for several mass exchange rates (Figure 11). The phase difference could be divided into two regions of dynamical behavior, a region of low phase difference (+70 to −70°) and a region of high phase difference, respectively. For the high difference region the slopes of the phase difference curve are independent of the mass exchange rate. The region of low phase difference (the region with a high local correlation coefficient) becomes wider with increasing mass exchange rate. When the mass exchange rate increases, the contribution of the low phase-difference increases, with the consequence that the correlation coefficient for the whole cycle increases.

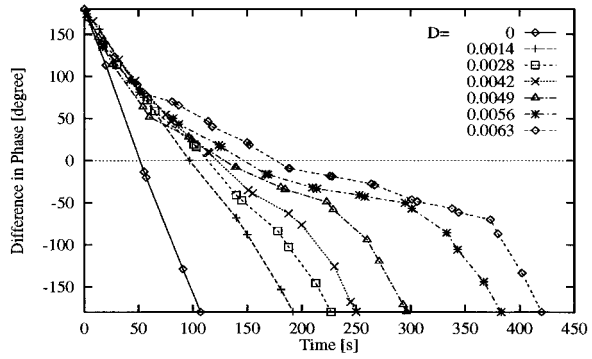

Figure 11. Experimental phase difference as a function of time for different mass exchange rates D at $\omega_2/\omega_1 = 0.65$.

When the modulation frequency tends to zero (the modulation period becomes infinite) in the quasiperiodic regime a collision of a saddle-node bifurcation with a torus is indicated, as described by Vance and Ross.[24] They studied bifurcations and Arnold tongues in a forced chemical oscillator and found that this bifurcation is generic for forced systems. In ordinary saddle-node bifurcations a stable node collides with a saddle point and then both disappear. At this point a special "saddle-node" singular point can be observed. A saddle-node can also lead to a periodic orbit if a third singular point, an unstable focus or an unstable node, is present. In that case a closed orbit will remain after the annihilation of the saddle-node point. This special kind of bifurcation is called **s**addle **n**ode **i**nifite **per**iod (SNIPER) bifurcation where the oscillations appear or disappear with finite amplitude but with an infinite period.[25,26] In our case we observe a SNIPER bifurcation of codimension two. The modulation period of the torus becomes infinite, and after the bifurcation a stable limit cycle remains.

This experimental observation is supported by calculation using the DOP model. Here, we observe the same behavior: a smooth expansion of a torus, the decrease of the modulation frequency of the quasiperiodicity, and the bifurcation to a stable limit cycle via a SNIPER bifurcation of codimension two.

Acknowledgment. We thank the Deutsche Forschungsgemeinschaft for partial support of this work.

References and Notes

(1) Winslow, R. L.; Cai, D.; Varghese, A.; Lai, Y.-C. *Chaos, Solitons Fractals* **1995**, *5*, 491.

(2) Marek, M.; Stuchl, I. *Biophys. Chem.* **1975**, *3*, 241. Marek, M.; Stuchl, I. *J. Chem. Phys.* **1982**, *77*, 1607

(3) Marek, M. *Spatial Inhomogenities and transient behaviour in chemical kinetics*; Manchester University Press: Manchester, 1988.

(4) Fujii, H.; Sawada, Y. *J. Chem. Phys.* **1978**, *69*, 3830.

(5) Nakajima, K.; Sawada, Y. *J. Chem. Phys.* **1980**, *72*, 2231. Nakajima, K.; Sawada, Y. *J. Phys. Soc. Jpn.* **1981**, *50*, 687.

(6) Crowley, M. F.; Epstein, I. R. *J. Phys. Chem.* **1989**, *93*, 2496.

(7) Boukalouch, M.; Elezgaray, J.; Arneodo, A.; Boissonade, J.; DeKepper, P. *J. Phys. Chem.* **1987**, *91*, 5843.

(8) Hauser, M. J. B.; Schneider, F. W. *J. Chem. Phys.* **1994**, *100*, 1058.

(9) Zeyer, K.-P.; Holz, R.; Schneider, F. W. *Ber. Bunsen-Ges. Phys. Chem.* **1993**, *97*, 1112.

(10) Holz, R.; Schneider, F. W. *J. Phys. Chem.* **1993**, *97*, 12239.

(11) Weiner, J; Holz, R.; Schneider, F. W.; Bar-Eli, K. *J. Phys. Chem.* **1992**, *96*, 8915.

(12) Hauck, T. Ph.D. Dissertation, University Würzburg, Würzburg, Germany, 1993.

(13) Zeyer, K.-P.; Münster, A. F.; Hauser, M. J. B.; Schneider, F. W. *J. Chem. Phys.* **1994**, *101*, 5126.

(14) Crowley, M. F.; Field, R. J. *J. Phys. Chem.* **1986**, *90*, 1907.

(15) Schneider, F. W.; Hauser, M. J. B.; Reising, J. *Ber. Bunsen-Ges. Phys. Chem.* **1993**, *97*, 55.

(16) Stuchl, I.; Marek, M. *J. Chem. Phys.* **1982**, *77*, 2956.

(17) Laplante, J. P.; Erneux, T. *Physica A*, **1992**, *188*, 89. Laplante, J. P.; Erneux, T. *J. Phys. Chem.* **1992**, *96*, 4931.

(18) Bar-Eli, K. *J. Phys. Chem.* **1984**, *88*, 3616.

(19) Sano, M.; Sawada, Y. *Phys. Lett.* **1983**, *97A*, 73.

(20) Schreiber, I.; Marek, M. *Phys. Lett.* **1982**, *91*, 263.

(21) Wang, X.-J.; Niccolis, G. *Physica* **1987**, *26D*, 140.

(22) Tyson, J. J.; Kauffman, S. J. *J. Math. Biol.* **1975**, *1*, 289.

(23) Degn, H.; Olsen, L. F.; Perram, J. J. *Ann. N. Y. Acad. Sci.* **1979**, *316*, 623.

(24) Vance, W.; Ross, J. *J. Chem. Phys.* **1989**, *91*, 7654.

(25) Noszticius, Z.; Stirling, P.; Wittmann, M. *J. Phys. Chem.* **1985**, *89*, 4914.

(26) Noszticius, Z.; Wittmann, M.; Stirling, P. *J. Chem. Phys.* **1987**, *86*, 1922.